Strategic Planning of Abort Trajectories for Manned Lunar Missions

Jillian Yuricich *

Georgia Institute of Technology, Atlanta, Georgia, 30332, United States

A resurgence in manned lunar missions is on the horizon with private space companies and nation states alike competing to be the first to return to the Moon since the Apollo program ended in 1972. Technology and mission planning abilities have expanded immensely in the almost half century of time that has elapsed since Apollo 11 first landed on the Moon. It is therefore necessary to evaluate and update how abort procedures should be strategized given the increase in volume of crewed missions planned for the Moon and beyond. This research seeks to investigate three abort strategies for space vehicles in orbit around the Moon and provide a high-level road map of options based on their fuel costs and time of flight to return to the Earth. By investigating previous historic works in combination with more recent research, this paper intends to capitalize on previous mathematical derivations and combine multiple abort strategies into a coherent simulation tool. It is expected that given the nominal trajectory of a circular lunar orbit, a specific abort strategy with options ranging from single to triple-impulse requirements can be selected as the optimal trajectory for a return to Earth. This research provides a high-level road map of contingency plans and fills a gap in understanding abort strategies from lunar orbit.

I. Nomenclature

FRT	=	Free Return Trajectory
LLO	=	Low Lunar Orbit
LOI	=	Lunar Orbit Insertion
$CR3BP$	=	Restricted Three-Body Problem
SLS	=	Space Launch System
SOI	=	Sphere of Influence
TEI	=	Trans-Earth Injection
TLI	=	Trans-Lunar Injection
ΔV	=	Applied change in speed of a maneuver, or impulse burn

II. Introduction and Motivation

Trips to the Moon may seem a distant relic of the Cold War, but the current resurgence in enthusiasm for lunar exploration spurred by commercial space companies around the world could mean a revival in crewed missions to the Moon and beyond to Mars. Companies like Blue Origin[a] and Space Exploration Technologies Corporation, or SpaceX[b], have both expressed their goals of returning to the Moon in some capacity as have multiple nation states like India, the United States, and China [1, 2].

Planning of such missions relies heavily on redundant systems and contingency plans including full mission aborts. A full mission abort refers to the abandoning of all nominal plans of the mission in order to return directly to Earth. Preparation for aborts early in the launch phase of a mission can be seen in current news

*Graduate Student, Georgia Institute of Technology, jyuricich@gatech.edu

[a]Bruce Dorminey. NASA's road back to the Moon may be via Bezos' Blue Origin, November 2017.

[b]Robin Seemangal. SpaceX's Mars plans hit a pothole. Up next: the Moon?, July 2017

with SpaceX's test of a pad escape abort system as well as Blue Origin's mid-flight capsule abort test. These abort systems are crucial during such volatile phases of flight. However, these systems test abort strategies for early within a mission and within the Earth's atmosphere. Further planning from the orbital mechanics perspective must also consider the need for a mission abort en route to or while near the Moon.

In order to best frame the abort solution, an understanding of mission planning and specifc orbit strategies to reach the Moon must be covered. While this research has applications relevant to Mars missions, this effort focuses solely on a lunar mission.

The simplest trajectory to the Moon from Earth is the Free Return Trajectory (FRT). The FRT option uses a Trans-Lunar Injection (TLI) burn, which slingshots the spacecraft on a figure eight path from the Earth to the Moon. The FRT strategy requires zero delta velocity (ΔV) to return to Earth, where ΔV refers to the change in velocity required to reach a new orbit. This means that if the vehicle were to have a reason to abort en route, an FRT trajectory would not require any ΔV to bring the vehicle back to the Earth; the spacecraft would simply coast in a figure eight shape. While an FRT requires the fewest burns and is therefore the least stressful on the vehicle propulsion system, it is more costly in fuel resources.

Another trajectory option is the hybrid trajectory, which uses less ΔV but requires two burns: one TLI burn to propel the vehicle toward the Moon from Earth and one Lunar Orbit Insertion (LOI) burn to place the vehicle in an orbit around the Moon. The TLI for a hybrid trajectory differs from that of an FRT mission in that it overshoots the Moon and does not create the same figure eight trajectory as seen with the FRT. Hybrid plans allow for the same space vehicle with the same fuel on-board to have some ΔV leftover to reach surfaces on the Moon unavailable to missions using a FRT strategy [3].

For missions where time is of no concern (mainly cargo or unmanned missions), the optimal fuel trajectory involves several orbits around the Earth in an "escape spiral" into a "Moon-capture spiral" [4]. Each of these trajectories requires a specific number of burns to complete. This statistic is important as it relies on a robust propulsion system capable of several restarts.

With this general picture in mind, it is clear that at some point in a manned mission, an LOI is necessary to prepare for descent to the Moon's surface. The underlying assumption for this work is that no matter the size or scope of the crewed mission, the vehicle will enter a circular orbit around the Moon should systems and the status of the crew remain nominal up until that point.

Together, this presents mission planners with the need to plan aborts from LOI for whichever trajectory is chosen. This location was selected for investigation because it represents the farthest away a vehicle will be from Earth. This research seeks to investigate trajectories for lunar mission aborts while in orbit around the Moon based on the state of the vehicle's orbit. As aforementioned, while this research intends to examine strategical abort planning for lunar missions, this work could also be applied to Martian missions, which have grown in popularity since the introduction of NASA's Space Launch System (SLS) [5, 6]. Relating this work to Mars missions would require an update on much of the underlying constants and orbit information as well as success criteria (final velocity after abort, position vector direction, etc.) but is otherwise highly relatable.

Because the lunar trajectory problem has existed for some time, there is an extensive amount of literature that focuses on minimizing fuel, energy or some combination of the three factors including works like Gong, et. al. which focus on invariant manifolds of the restricted three-body problem [7]. More modern works highlight the importance of lunar ascent and rendezvous for landers as seen in Sostaric and Merriam's work [8]. A variety of publications seek to address the guidance and navigation concerns of an abort and some investigate aborts and strategies from the Apollo era [9]. Especially studied is the infamous Apollo 13 mission by recreating its trajectory after aborting the landing mission and drawing conclusions from a vehicle and mission design perspective for future contingency operations [10].

With respect to mission abort trajectories, Gunther's influential 1966 work discusses one- and two-impulse transfers from a lunar parking orbit (LPO) to a non-planar, hyperbolic asymptote, presumably a hyperbolic orbit back to Earth in a maneuver otherwise known as a Trans-Earth Injection (TEI) [11]. As well, Edelbaum's 1971 study on three- and four-impulse transfers provides an optimal minimum impulse solution between a circular orbit and hyperbolic velocity vector at infinity[12].

While these historical and modern works alike plan strategies around multiple numbers of impulse burns for aborting a mission, none take into account the optimal strategy to minimize time to return to Earth. If an abort takes place, whether it be due to system failures or health reasons within the ranks of the crew, time is the most important resources the team will have.

However, the current state of space exploration has a growing number of involved parties and updated

technologies. It is also important to consider how new rocket engine technologies, vehicle guidance, navigation, and control systems, and autonomous features play into the decision to abort a mission. Certain scenarios could arise where fuel is more important than a short trip home. For instance, an aborted mission due to unforeseen vehicle failures could provide an opportunity for opportunistic science conducted in orbit around the Moon or observations in the stars on the route back to Earth should the health of the crew allow it. Many of these scenarios are addressed at the end of this work. This research contributes (1) a combined analysis of mulitple abort strategies using various historical derivations to compare fuel required and time of flight and (2) a simulation of the various resultant trajectories from the three abort strategies that incorporates an EKF estimator and uncertainties due to engine misalignment and thrust magnitude errors.

III. Theory and Background

This section provides an outline of the underlying dynamics and derivations used to build simulations of the abort impulse scenarios for lunar missions. The overarching strategy of this research was to observe the results of three different types of abort methods. The abort strategies were broken up into three options:

1. **Single-impulse abort:** Execute a single burn of the vehicle's engine to place vehicle on an orbit directly back to Earth (Section III.A.1).
2. **Two-impulse abort:** Execute two engine burns where the vehicle burns once in orbit around the moon and again at the edge of the SOI of the moon (Section III.A.2).
3. **Three-impulse abort:** Execute three engine burns over the course of an orbit and a half around the moon before leaving the SOI of the moon and heading back to the Earth (Section III.A.3).

The key factors at play for mission aborts include fuel costs to reach a desired ΔV, time it takes for the vehicle to return to Earth, quality of the engine on-board the vehicle to handle multiple restarts if necessary, and size of the mission vehicle. While this research focuses on fuel costs and time of flight, the secondary factors of relighting an engine and size of vehicle may limit which strategy should be chosen. For example, if an abort happens due to vehicle hardware or software malfunctions, it may not be safe to rely on the engine for multiple burns. As well, if the vehicle is incapable of reaching a certain value of ΔV for whatever reason, it may rule out an abort method that is more expensive with respect to fuel costs.

The rest of this section focuses on the mathematical expressions derived to calculate the fuel cost of an abort strategy.

A. Abort Impulse Calculations

Two main sources were used as a basis for deriving abort strategies across the one-, two-, and three-impulse trajectories [11, 12]. This section is not an exhaustive list of the equations provided by these sources but rather a description of the most important values for this research. Each of the following subsections derives the equations used to calculate the cost of each maneuver for single-, double-, and triple-impulse strategies with respect to a varying K value, which is the end velocity V_∞ normalized by the circular velocity of the vehicle about the moon, V_{circ}. This method is adapted from how Gunther solved for the ΔV cost of each burn for one- and two-impulse maneuvers. Some adjustments were then required of Edelbaum's method because while similar in end goals, each author had very different results that required reconciling to be comparable. Each individual preliminary result is shown in Section IV while the results of all three strategies combined are compared in Section V.

1. One-Impulse Abort

Gunther provided derivations for an optimum one- and two-impulse transfer from lunar orbit based on minimizing ΔV cost [11]. Gunther's derivations focus on the parameter K, which is the vehicle velocity after the abort normalized by the circular velocity from when in orbit around the moon. Gunther also uses the parameter $\Delta V'$, or normalized ΔV. The expressions are as follows.

$$K = \frac{V_\infty}{V_{circ}} \tag{1}$$

$$\Delta V' = \frac{\Delta V}{V_{circ}} \tag{2}$$

Gunther's key derivation involved the use of ω, a parameter with no geometric meaning, but whose root is used to calculate various geometrically relevant values such as flight path angle, eccentricity, and most importantly, the required ΔV for the maneuver executed at perigee. The full derivation for ω can be found in Gunther's 1966 paper [11].

Figure 1 shows the geometry of the maneuver. In Figure 1, the moon is located at the center point and the circular orbit around the moon is represented by the solid line. The vector $\bar{v}^-$ represents the trajectory before the impulse where the velocity vector is tangent to the elliptical orbit. Immediately after, the velocity vector $\bar{v}^+$ shows the new velocity vector which puts the space vehicle on a trajectory towards the Earth in the $\bar{V}_\infty$ direction. This figure is adapted from multiple sources [11, 13].

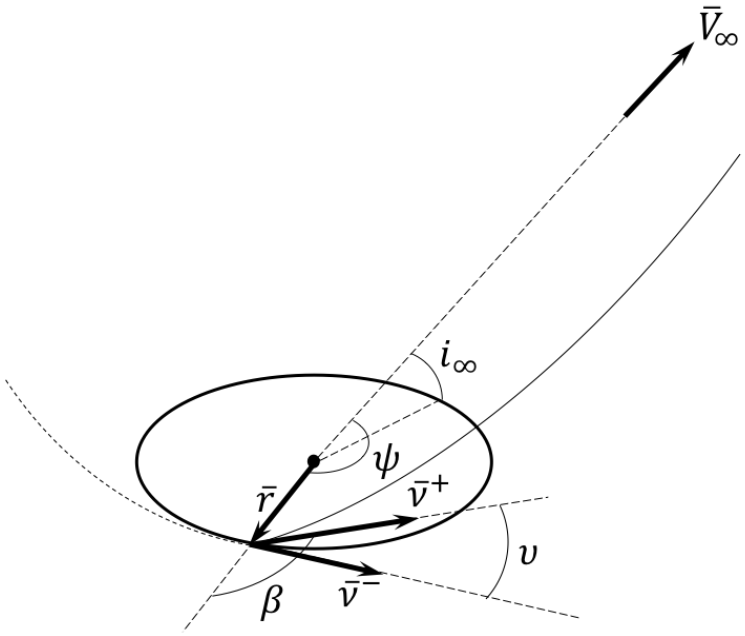

Figure 1: Geometry of a one-impulse maneuver out of the orbit of the moon.

The ω expression Gunther derived is below and is a function of the value K and i_∞. K must be chosen by the trajectory team for the mission based on where the vehicle is located around the moon from which an i_∞ can be solved. This is one of the pitfalls of this research, which is further addressed in Section V. For this reason, all of the results provided vary with K such that users are given the opportunity to see just how the end results are affected.

$$\omega^4 - K\omega^3 - Ksin^2(i_\infty)\omega - sin^2(i_\infty) = 0 \tag{3}$$

With this optimal ω calculated, it is immediately found that:

$$\frac{\Delta V_1}{V_{circ}} = \sqrt{K^2 + 3 - 2\sqrt{(1 + K\omega - \omega^2)(2 + K\omega)}} \tag{4}$$

Equation 3 is the main source of results for the single-impulse abort fuel costs. However, Gunther provides much more information. The ω is also used to calculate the compliment of the flight path angle after the impulse, which can be expressed as:

$$cos(\beta) = \frac{\omega - K}{\sqrt{K^2 + 2}} \tag{5}$$

The eccentricity after the impulse for the hyperbolic trajectory is given:

$$e^2 = (K^2+1)^2 - K^2(K^2+2)cos(\beta) \tag{6}$$

Using e and β, two angles can be calculated to quantify the changes in direction for both the velocity and position vectors. This φ angle represents the angle between the position vector at the impulse and the escape asymptote and is computed as:

$$\varphi = cos^{-1}\left(\frac{-1}{e}\right) - cos^{-1}\left[\frac{1}{e}\left(\frac{e^2-1}{K^2}-1\right)\right] \tag{7}$$

As well, the equation for ν, the angle between the velocity vector immediately prior to the impulse and the new velocity vector after the impulse is:

$$cos(\nu) = sin(\beta)\sqrt{1 - \frac{sin^2(i_\infty)}{sin^2(\varphi)}} \tag{8}$$

The values of β, e, ψ, and ν provide additional information to the user for converting normalized values of velocity into velocity and position vectors.

2. Two-Impulse Abort

With larger requirements of i_∞, single impulse aborts become very expensive with respect to fuel [11]. Multiple maneuvers decrease the amount of fuel required for a high i_∞ abort by breaking up the abort into multiple stages, which overall, save on fuel. However, when executing multiple impulses, a vehicle is required to have an engine with reliable re-light abilities.

For a two-impulse abort, the first impulse increases the orbital energy of the vehicle on an intermediate low-energy escape trajectory. The second impulse occurs at the edge of the moon's SOI where a burn completes the final plane change requirements and puts the vehicle on a final departure trajectory. The trajectory can be see in Figure 2 derived from [11] and [13].

As specified in section A1, the original circular orbit about the is the solid-line where the moon is represented by the center point. The first impulse maneuver is the same as the maneuver from Figure 1 except the final direction of this impulse is represented by the vector $\bar{V}_{\infty_1}$. To reach the $\bar{V}_\infty$ and the final direction of the abort, the vehicle executes a second impulse, which is shown at the moon's SOI as $\bar{v_2}^+$. Here, ψ shows another angle change along with the final inclination change of i_2.

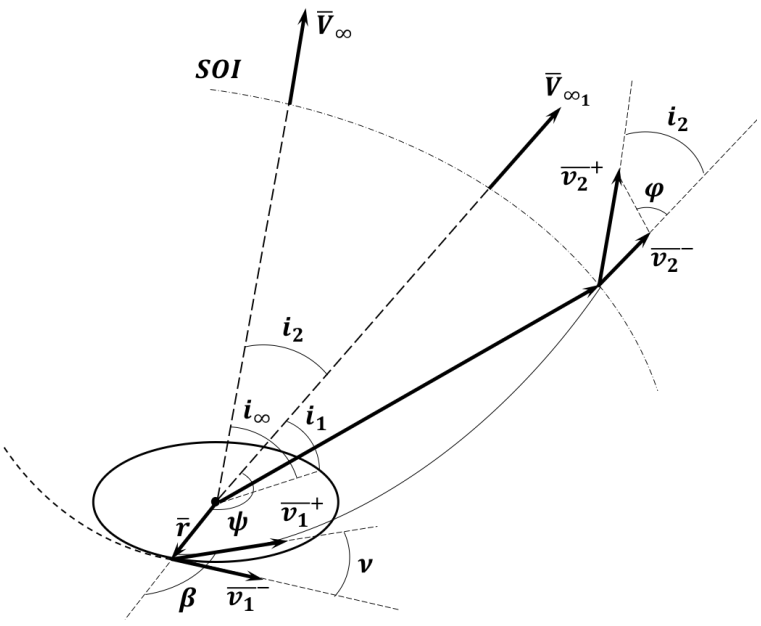

Figure 2: Geometry of a two-impulse maneuver out of the orbit of the moon [13]

.

Again, Gunther's derivations rely on normalized, non-dimensional velocities, this time with an additional term referred to as K_1 that encapsulates the first abort where:

$$K_1 = \frac{V_{\infty 1}}{V_{circ}} \tag{9}$$

Similar to the single-impulse strategy, a polynomial with respect to ω is derived and the roots of which are used to calculate the remaining pertinent parameters.

$$\begin{aligned} 4K_1^2\omega^6 + 4K_1\omega^5 + \left(1 - 16K_1^4\right)\omega^4 + 2K_1\left(1 - 20K_1^2 + 8K_1^4\right)\omega^3 ... \\ ... + \left(1 - 19K_1^2 + 40K_1^4\right)\omega^2 + 2K_1\left(8K_1^2 - 1\right)\omega + K_1^2 = 0 \end{aligned} \tag{10}$$

For values $K > 1.076$, there are no positive roots to this polynomial, and therefore this paper will not consider those value of K. With $K < 1.076$, there are two positive roots, the minimum of which constitutes the global fuel-optimal maneuver [13]. With this minimum ω in hand, one can calculate the initial inclination change from the first impulse burn. Note that if this i_1 is larger than i_∞, then the single impulse procedure is a better solution than the two-impulse one.

$$sin^2(i_1) = \omega^3\left(\frac{\omega - K_1}{1 + K_1\omega}\right) \tag{11}$$

With K_1 and i_1 known, these values can be used in the equations from section A1 (specifically Equations 7 and 8) to determine the velocity and position angle changes as well as Equation 4 to determine the normalized ΔV_1. A new value of φ (which must be less than $\frac{\pi}{2}$) is calculated from the following geometric relation:

$$cos(\varphi) = \frac{V_{circ}}{\Delta V_1}\left(K_1 - \omega\sqrt{\frac{1 + K_1\omega - \omega^2}{2 + K_1\omega}}\right) \tag{12}$$

From here, the second impulse ΔV_2 can be calculated using the following equation:

$$\frac{\Delta V_2}{V_{circ}} = \sqrt{K^2 + K_1^2 sin^2(\varphi)} - K_1 sin(\varphi) \tag{13}$$

Recall, K is the normalized V_∞ whereas K_1 is the normalized $V_{\infty 1}$ from the first of the two impulses. Finally, the last inclination change i_2 is found through the following expression:

$$i_2 = \varphi - sin^{-1}\left[\frac{K_1}{K} sin(\varphi)\right] \tag{14}$$

The previous equations must all be used to solve for $K1$ as a function of K and i_∞ numerically, according to Robinson/Geller[13]. Their work provides an approximation for K_1 in Section IV.B, which for the scope of this research, is an appropriate estimate to use.

3. Three-Impulse Abort

Edelbaum provided an optimal escape from circular orbits that use three- or four-impulses. This work focuses on his derivation of three-impulse maneuvers and neglects his higher order terms, which are addressed in Edelbaum's work but not derived explicitly. The trajectory of such a maneuver is in Figure 3.

In Figure 3, the three-impulse maneuvers are seen at each half orbit around the moon, which is represented by the center point. This maneuver takes place over one circumvention of the moon, thereby being the most time consuming of the abort options. This figure was adapted from Edelbaum [12].

The derivation begins with the definitions of eccentricity of the escape trajectory hyperbola e, the minimum angle between the asymptote and the circular orbit plane given as θ, as well as the calculation of i, which is the angle (0 to $\pi/2$) between the plane of the third impulse and the velocity asymptote. Both expressions for e and i are given as:

$$e = 1 + \frac{R_p V_\infty^2}{\mu} \tag{15}$$

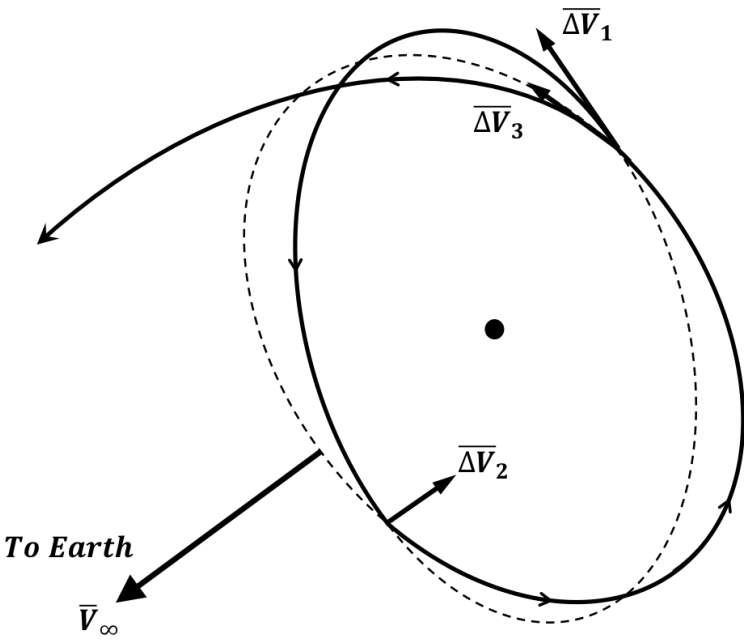

Figure 3: Geometry of a three-impulse maneuver out of the orbit of the moon [12]

.

$$sin(i) = \frac{esin\theta}{\sqrt{(e^2-1)}} \tag{16}$$

For the first impulse, the magnitude of the ΔV is given as the following expression where R_a is the apoapsis radius of the first and second transfer ellipses.

$$\Delta V_1 = \sqrt{\frac{2\mu}{R_0}}\left[\frac{1}{2} - \frac{1}{2}\frac{R_0}{R_a}\right] \tag{17}$$

The small plane change derived from this first maneuver can be quantified as:

$$\beta_1 = \frac{R_0 sin(i)}{R_a}\sqrt{\frac{2R_p}{R_0 + R_p - 2cos(i)\sqrt{R_0 R_p}}} \tag{18}$$

The inclination change derived from the first impulse is:

$$i_1 = \frac{\left(\sqrt{2}-1\right)R_0\sqrt{R_p}sin(i)}{R_a\sqrt{R_0 + R_p - 2cos(i)\sqrt{R_0 R_p}}} \tag{19}$$

Once the vehicle reaches nearly the opposite position in orbit (i.e. half an orbit around the moon), the second impulse burn occurs to provide the majority of the plane change required and lower the periapsis. The magnitude of this ΔV is:

$$\Delta V_2 = \frac{2\mu\sqrt{R_0 + R_p - 2cos(i)\sqrt{R_0 R_p}}}{R_a} \tag{20}$$

Finally, the third impulse, which takes place at the same location as the first, has a ΔV and i_3 of:

$$\Delta V_3 = \sqrt{\frac{2\mu}{R_p} + V_\infty^2} - \frac{2\mu}{R_p}\left[1 - \frac{R_p}{2R_a}\right] \tag{21}$$

$$i_3 = \left(1 - \sqrt{\frac{2}{\sqrt{e+1}}}\right)\beta_{32} \tag{22}$$

$$\beta_{32} = \frac{R_p}{R_a}\left[\frac{\sqrt{R_0}sin(i)}{\sqrt{R_0 + R_p - 2cos(i)\sqrt{R_0 R_p}}}\right] \tag{23}$$

These expressions are much more direct methods of solving for either the single- or two-impulse burn solutions. However, they require much more knowledge of the scenario with respect to the lunar orbit rather than the use of normalized terms as seen in the previous derivations. This is an important note for comparing the strategies.

IV. Impulsive Abort Strategy Simulation

Each abort strategy derivation from Section III.A formed the basis for writing three simulations. MATLAB was used for this work. The simulations for each type of abort was first written individually as functions. A script was used for each strategy to investigate trends within each. The final simulation incorporates all three functions into one wrapper with each of the abort functions used.

A. One-Impulse Abort Simulation

A single-impulse abort was modeled using the aforementioned dynamics from Section III.A.1. A variety of K values (selected based on recommendations within Gunther's work) were selected between zero and one to compare a variety of V_∞ that are required for the escape. In this particular simulation, the Gunther polynomial equation (Equation 3) was developed as a function in MATLAB used to calculate the optimal ω for a given K.

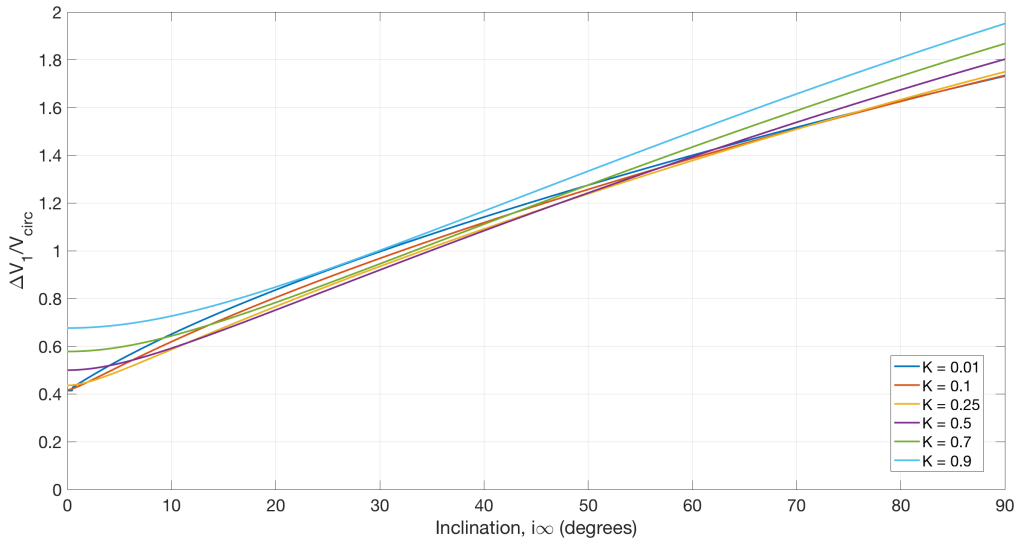

Figure 4: Non-dimensional ΔV_1 with respect to inclination for multiple K values from Reference [13].

Using this ω, a variety of other parameters were calculated for the resulting trajectory after the single burn. Figure 4 displays the relationship between ΔV_1 and required inclination, i_∞ for the trajectory. If not well understood prior to this investigation, Figure 4 makes clear that single-impulse maneuvers quickly become expensive. For any value of K, an inclination i_∞ over 35-degrees requires a ΔV larger than its circular velocity in orbit around the moon.

The benefits of a single-impulse abort, however, cannot be understated. One burn is the least complex option, which is especially important if the mission abort occurred as a result of unresponsive or debilitated

on-board systems. In an emergency, the priority is to save the crew and return the vehicle safely. Conserving fuel is no longer a necessary objective in the case of an abort. Because of this, if the vehicle has the capacity to perform a single impulse abort, they should. However, this capacity can change throughout a mission as the vehicle burns fuel to orbit the moon. Therefore, there is a time threshold based on the fuel stores aboard the vehicle where a single-impulse abort maneuver is no longer viable.

B. Two-Impulse Abort Simulation

The two-impulse strategy was slightly more complex to simulate compared to the one-impulse maneuver. Because of this, an single trial was run successfully rather than provide a trend across inclinations similar to the results in Figure 4. This single trial confirmed that the code was working, but from this, the complex relationship between K and K_1 arose. Figure 5 provides an estimation for how to choose K_1 given a desired K and i_∞.

Because this abort strategy requires two different K values, one for each burn, a comparison was required to understand how they relate. The value of K is used to calculate the first ΔV burn in the exact same manner as the one-impulse method. For the second burn, both K and K_1 are needed. Figure shows how K_1 trends with i_∞ for specific values of K. While Gunther used multiple complex methods to numerically calculate the non-linear expressions of K_1 as a function of i_∞ and K, this work aimed to save time and used approximations derived from the same equations to capture the linear trends.

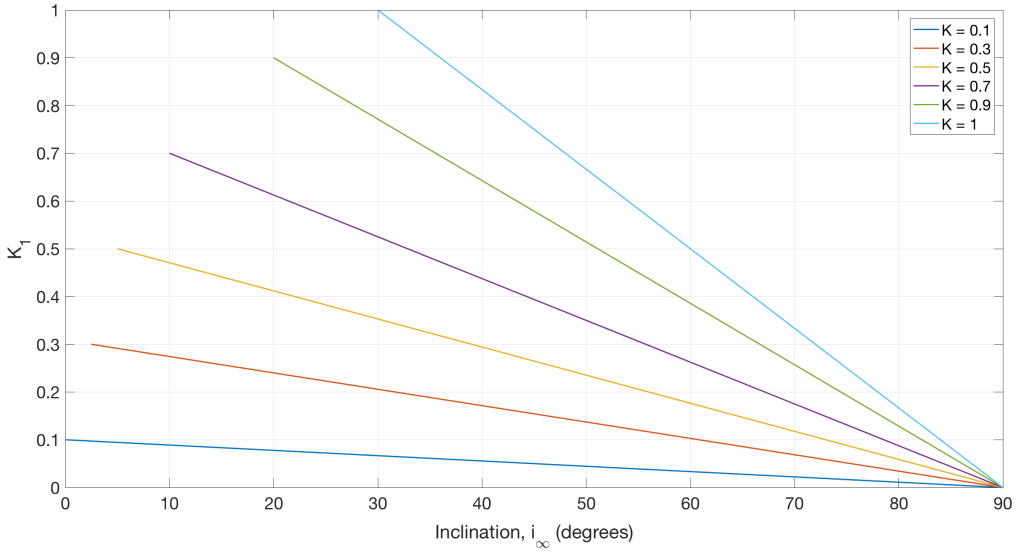

Figure 5: K_1 relationship with inclination, i_∞, and K that ends with $K_1 = K$, where a single impulse maneuver is the minimum for fuel consumption.

As well, Figure 5 terminates to the left for all lines where $K_1 = K$ as evidenced by most of the trends failing to reach the y-axis. This is because if $K_1 = K$, the first impulse of a two-impulse maneuver equals the ΔV of the sole burn of a single-impulse maneuver. It would nonsensical to then do another burn, which is obviously higher in fuel costs, and therefore makes the single-impulse burn the most efficient for that specific scenario.

As previously stated, the increased complexity of the two-impulse burn derivations and calculations make recreating a similar plot to Figure difficult. However, for given values of K and an explicit i_∞, the simulation is able to predict the total ΔV required for the maneuver.

C. Three-Impulse Abort Simulation

Because Edelbaum's derivations were so vastly different from Gunther's methods, the simulation built was adjusted immensely to be comparable to Gunther's comparison of non-dimensional ΔV to i_∞. The result was that several factors including circular orbit radius about the moon, apoapsis and periapsis radii during

the transfer, and final hyperbolic velocity would need to be toggled to show the effects they had on the cost of the three-impulse maneuver. This is much different from the equations provided by Gunther to calculate the normalized ΔV.

For example, varying escape velocity magnitude, apoapsis radius, and periapsis radius all create different trends for normalized ΔV. However, all of the trends are similar to the single-impulse results from Section IV.A in that they have monotonically positive, relatively linear slopes.

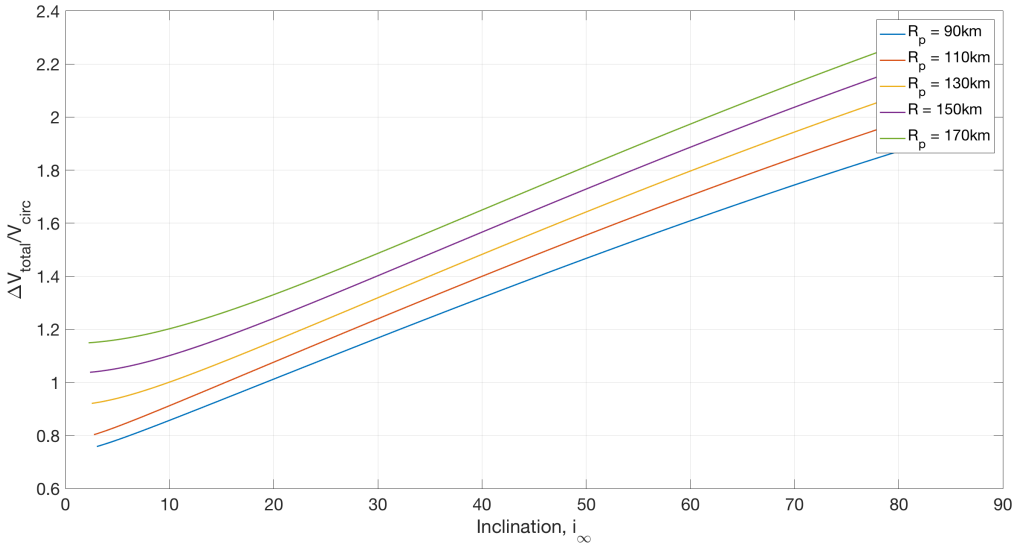

Figure 6: For various R_a values, the overall ΔV changes dramatically in a very similar trend and magnitude as the single-impulse maneuver.

With changing R_p values as seen in Figure 6, the requirements for ΔV are very high, at times much higher than the single-impulse requirements, rendering the three-impulse strategy useless. This experiment made clear that choosing a nominal orbit around the moon as well as other factors to describe the abort scenario (R_a, R_p, etc.) is immensely important for minimizing fuel consumption. In Figure 7, the final velocity also straddles a great range of ratios for the total ΔV.

These types of trends with respect to varying R_a and V_∞ are only possible to identify with the Edelbaum method considering Edelbaum's derivations rely on specific values of R and V versus Gunther's normalized velocities and ΔVs. Figures 6 and 7 show that R_p is more sensitive to changes that can impose a much higher fuel penalty whereas changes to V_∞ span a smaller range of normalized ΔVs.

Because the slope of the trend lines in Figure 6 were much steeper than those of Figure 7, it was clear that R_p (as well as R_a) would be the more important factor to consider when deciding the final trajectory for a three-impulse abort. More discussion on this trend and its implication is explained in Section V.

V. Results and Discussion

The key findings from this research can best be displayed by a few plots. By overlaying each abort strategy's curve for normalized ΔV versus K value, the minimum for each value of K can be found. For the reader's convenience, a few equations (Equations 1 and 2) are recalled here from previous sections.

$$K = \frac{V_\infty}{V_{circ}}$$

$$\Delta V' = \frac{\Delta V}{V_{circ}}$$

While this plot only takes into account to fuel costs, it is possible to draw several conclusions regarding how a mission director may choose which abort strategy is appropriate for any given scenario. There are three curves in Figure 8 that overlay each other for K values between zero and one. These curves each represent

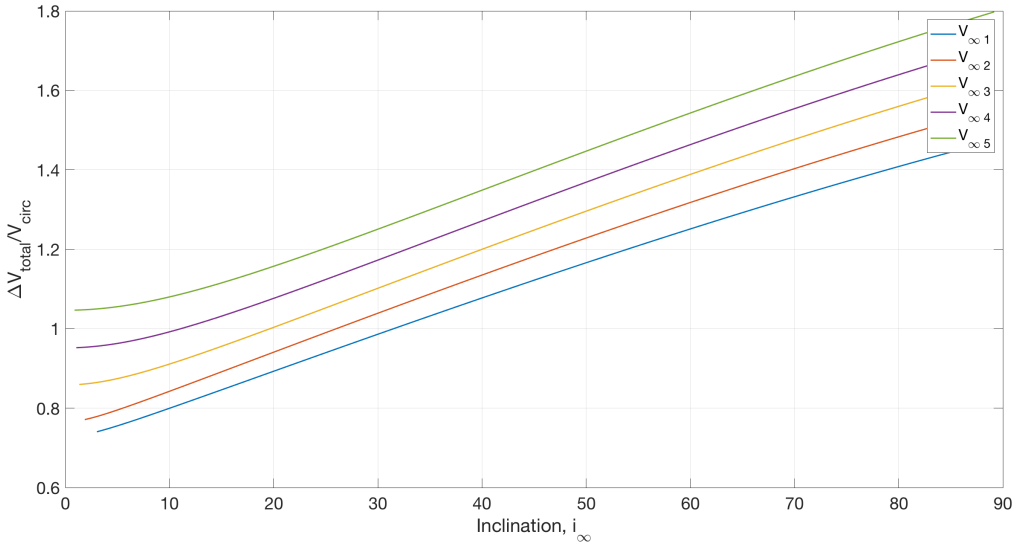

Figure 7: While similar in shape and trend, the normalized ΔV values are much smaller than those of Figure 6 and similar to Figure 4.

single-, double-, and triple-impulse abort maneuvers. The black dotted line represents the minimum $\frac{\Delta V}{V_{circ}}$ required from the K selected by the mission planner. It can be seen that this line covers all three impulse curves at one point or another.

The solid blue line shows single-impulse maneuvers in a curve that arcs between roughly 1.16 to 1.28 $\frac{\Delta V}{V_{circ}}$. Frankly, given the lessons Gunther communicated whereby single impulses to return to Earth are the most expensive, this was a much lower range than expected.

For the two-impulse maneuver, the curve starts high around 1.44 $\frac{\Delta V}{V_{circ}}$, but dips at its lowest to about 1.12. This curve shows how efficient the two-impulse maneuver is at higher K when it is necessary to achieve a high V_∞ for the return to Earth.

Finally, the three-impulse fuel cost is almost a mirror of the two-impulse maneuver where the curve starts at 1.12 $\frac{\Delta V}{V_{circ}}$ but grows very quickly peaking at 1.43. For this plot, R_a was 300 kilometers and R_p was 111.1 kilometers. This was the most unexpected trend of the results in Figure 8 in that it grew the quickest of all the impulse strategy options. It was hypothesized that the most efficient abort with respect to fuel would be the one with the most burns. However, Figure 8 shows that simply is not the case. It can be seen that the three-maneuver option is only efficient at low values of K.

The trend from the three-impulse strategy was unexpected, so more investigation was necessary. As aforementioned, a nominal orbit about the moon was needed to use Edelbaum's derivations, but the method also relied on choosing the apoapsis and periapsis for the transfer. According to historical data from Apollo missions, the circular orbit about the moon was at an altitude of 60 nautical miles or 111.1 kilometers [14]. With this in mind, the variable R_0 was set to 111.1 kilometers with the periapsis R_p also set to 111.1 kilometers as well (the decision surrounding the value of R_p had little historical data to rely on). It was then necessary to determine a value for the apoapsis, R_a. While a value of 300 kilometers was used in Figure 8, a study was completed resulting in Figure 9 showing that with varying R_a, the ΔV cost changed over K for a three-impulse maneuver.

Because there is little existing literature that describes the apoapsis and periapsis distance values a vehicle should reach for a three-impulse abort around the moon, it leaves the trajectory up to the designer whereby higher apoapsis values reached uses less fuel, a trend easily seen in Figure 9. However, with very high apoapsis values comes a penalty in time of flight. The farther out the vehicle orbits during the abort, the longer it takes to reach the Earth.

From the plot, it is clear that the trend lines get closer together and the fuel penalty becomes less and less as R_a grows. While the difference between small values of $\Delta V/V_{circ}$ cannot be written off entirely (due to the fact they are normalized by V_{circ} which is a large value), for the purposes of this research, $R_a = 300$

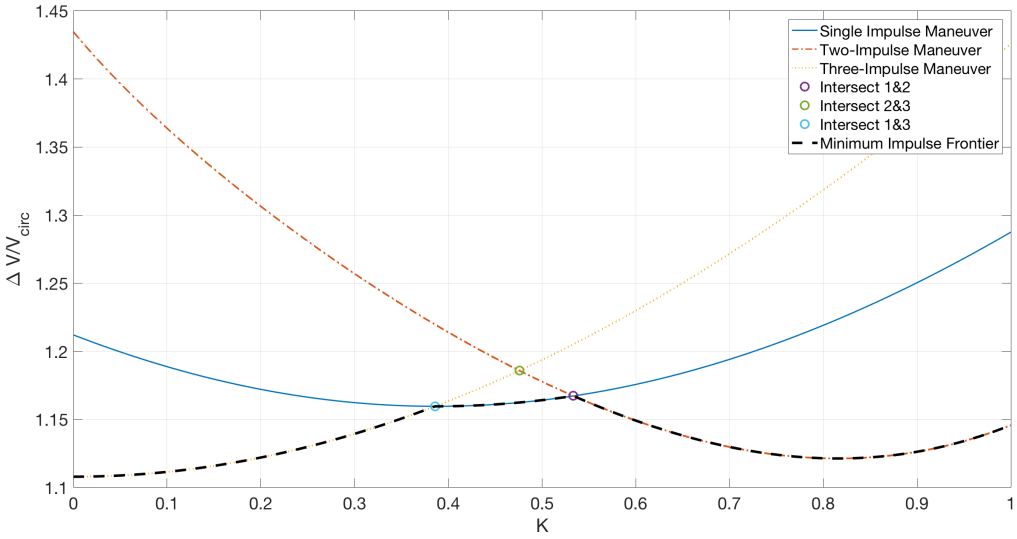

Figure 8: Display of all impulse abort options (1, 2, and 3) for leaving lunar orbit and returning to Earth.

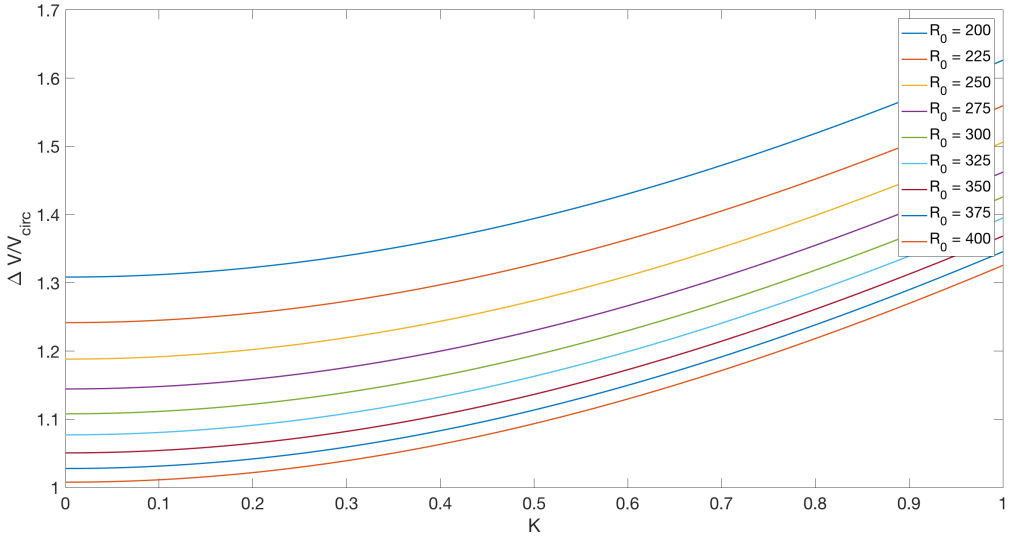

Figure 9: Analysis of the three-impulse maneuver cost in ΔV by varying the value of R_a with a constant .

kilometers was chosen as it reflects a mid-range value and where the trend lines begin collapsing.

Because the value of R_a is highly variable from mission to mission, it was important to find which value of apoapsis makes the three-impulse maneuver no longer viable as a maneuver option for any $0 < K < 1$. Further, this means finding the value of R_a where the three-impulse maneuver is the worst option for fuel cost of all the impulse strategies across all values of $0 < K < 1$. It was found that at a radius of about $R_a = 238$ kilometers, three impulses are the least efficient option; Figure 10 makes this clear.

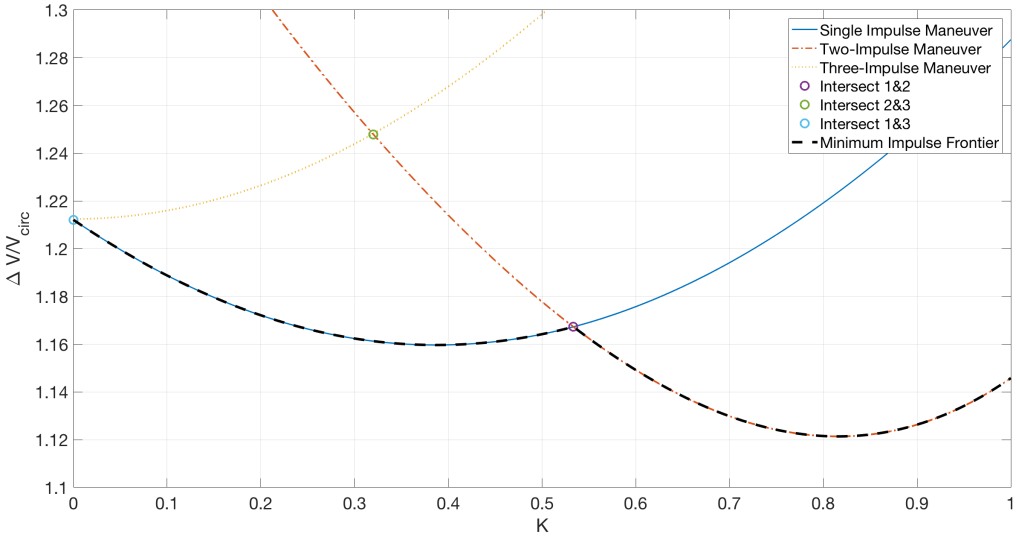

Figure 10: At an apoapsis of 238 km, the three-impulse maneuver option is no longer viable.

Any apoapsis lower than 238 kilometers ensures that the three-impulse maneuver is the highest cost fuel option at a given K. Figure 10 shows what the overlaid impulse curves look like when $R_a = 238$ kilometers for the three-impulse maneuver. The black dotted line that tracks the minimum normalized ΔV required shows that for no values of K is the three-impulse strategy a minimum.

However, there also exists a value for R_a where the three-impulse maneuver costs the least amount fuel than any other strategy across all values of $0 < K < 1$. This maneuver should not be employed if the crew are in danger as the time of flight would be much higher than a "nominal" three-impulse maneuver with a value of R_a near 300 kilometers. Yet, the situation could arise where a crewed vehicle aborted would like to get some science mission done while in orbit around the moon where a longer time of flight is desired. In this scenario, a three-impulse maneuver which, for all values of $0 < K < 1$, is the minimum fuel cost occurs at a $R_a = 995$ kilometers. Figure 11 shows this where the three-impulse trend line and the black, dashed minimum line follow the same curve.

From this investigation into the affects of R_a on the three-impulse maneuver, it is clear that this strategy has the potential to be a great catch-all for non-emergency aborts, however narrow that category might be. This catch-all only works though if the engine aboard is reliable enough to make these three impulses.

As mentioned in Section III.A.1, a caveat in the use of K is an important limiter of this research. Gunther's derivations use the K value as a user controlled input, which requires knowledge of the vehicle's location in orbit around the moon. This research was initially intended to weigh the cost of aborting from lunar orbit by factoring in both fuel costs and time of flight with the goals of minimizing both. Unfortunately, Gunther's estimations do not take $\bar{r}$ or $\bar{v}$ vectors of position and velocity around the moon into account. Once work of this research was fully underway, it became clear that the derivations for fuel cost left out information regarding the space vehicle's specific position around the moon and normalized the data by the vehicle's current velocity about the moon (represented by both V_{circ} and $\bar{v}^-$).

In the end, because the results are based on a varying K, the plots and descriptions provide insight generally into how V_∞ affects the fuel costs of an abort procedure. A user could then calculate K given their desired end velocity vector to return to Earth. From here, the plots and results of this work would show which abort strategy is the best option. This varies from the initial goals of this research, which were to provide a more end-to-end description of how to abort away from the moon given a position in lunar orbit.

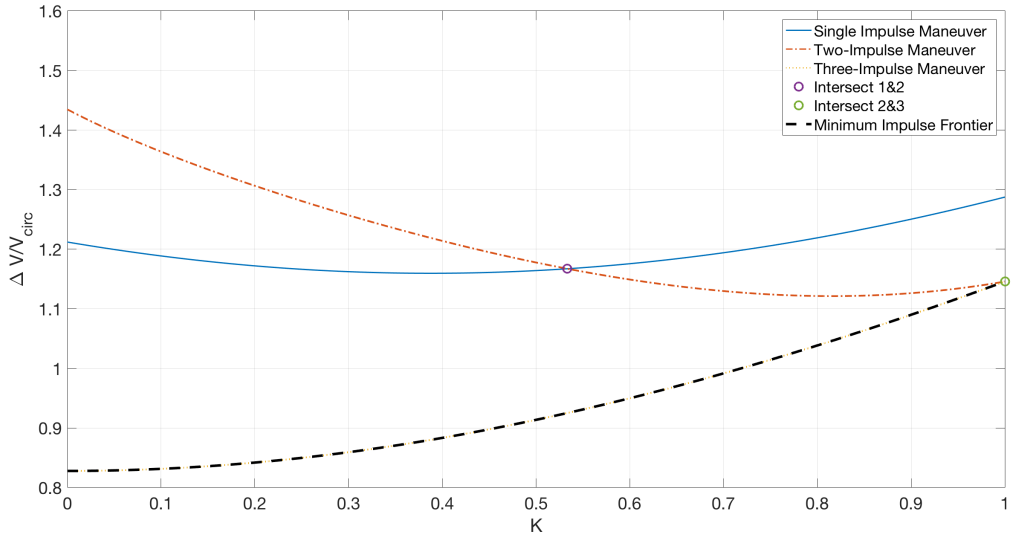

Figure 11: At an apoapsis of 995 km, the three-impulse maneuver option requires minimum fuel across values of $0 < K < 1$.

However, because the results are still general, and the simulation built allows for users to input their specific orbit parameters, it simply solves the problem in a manner different than originally planned.

When considering the time of flight aspect of this research, it was made clear that generally, the less impulses meant shorter time of flight. This is mainly because of the strategy with which the impulses use to return to Earth. One-impulse abort strategy is essentially a direct abort with no slingshot or extra maneuvering. For two-impulse aborts, the vehicle continues to orbit the moon after its first impulse before finally one last burn at the SOI of the Moon. Finally, the three-impulse abort relies on nearly a full lunar orbit around the Moon before returning to Earth. At an altitude of 111.1 kilometers above the Earth, a full orbit takes almost exactly two hours to complete. It is easy to then infer that each added engine burn adds time to the return. With this in mind, Figure 12 was developed to communicate areas where each abort method is most efficient.

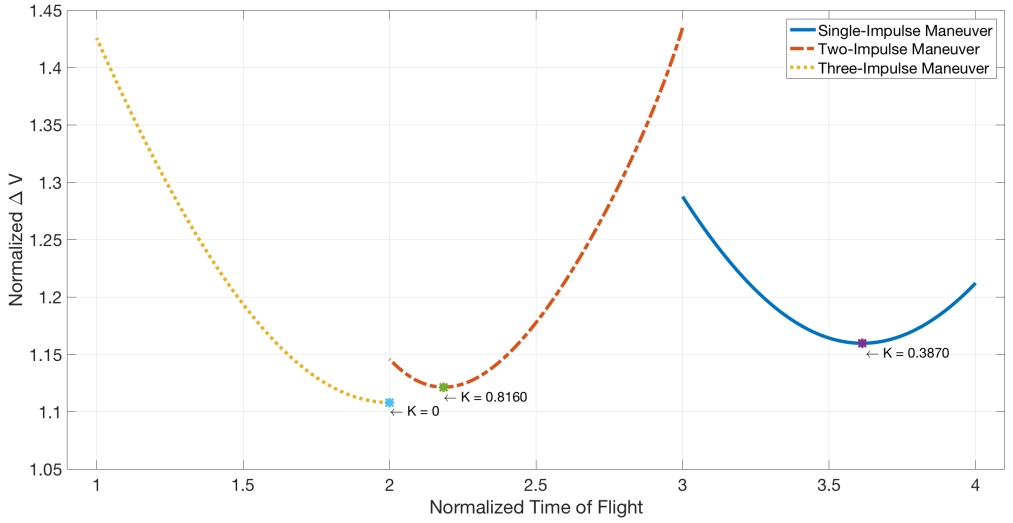

Figure 12: Given that more maneuvers means longer time of flight, the optimized solution for each maneuver type is given whereby the most efficient value of K for each abort strategy is shown.

In Figure 12, the time of flight for each maneuver has been normalized by the minimum time of flight overall where each strategy has been plotted for its time of flight and corresponding normalized ΔV cost. This plot reveals the value of each K that is the most optimized solution for the given abort strategy considering both factors of time of flight and fuel costs. Table 13 lists the values again.

Optimized K Values	
Single-Impulse Abort	$K = 0$
Two-Impulse Abort	$K = 0.8160$
Three-Impulse Abort	$K = 0.3870$

Figure 13: Values of K optimized for each abort strategy. The three-impulse strategy uses the same R_a and R_p values as Figure 8.

The key findings from Table 13 and Figure 12 are that each method has a "sweet spot". Starting with the three-impulse abort method, it is clear here that the smaller the K value the better. Meanwhile for two-impulses, mid-range K values work best whereas the one-impulse strategy favors higher values of K. All of these analyses together provide a better understanding of how abort strategies differ and give mission planners guidelines on which to choose given their particular abort scenario.

VI. Error and Uncertainties Analysis

Pivoting from the impulse cost analysis sections of this research, a new analysis was conducted to model trajectories within the Earth/Moon system and identify sources of error that may propagate throughout the trajectory. This section focuses on the truth that no pieces of hardware work to exact specifications and that the realities of spaceflight encompass some amount of uncertainty. The following work looks to identify certain sources of uncertainties when propagating trajectories forward through time over the course of an abort maneuver starting from the Moon.

The first section explains the quantification of the uncertainties in a space vehicle system and are followed by a section explaining the dynamics of the Circular Restricted Three-Body Problem (CR3BP).

The final sections of this report document a comparison between the simulated vehicle trajectory from the Earth to the Moon and a trajectory estimation using an Extended Kalman Filter. The simulation, regarded as "truth", takes into account engine mounting errors and thrust magnitude errors while the EKF propagates the trajectory and updates it using range measurements from Earth. A comparison and discussion of these trajectories is in Section VI.C.

A. Sources of Uncertainty in Abort Maneuvers

One of the main sources of uncertainty with respect to spaceflight hardware is from the rocket engine. When mounting the engine, it is estimated that it is possible to point the hardware to within one half-degree of accuracy. The variability in exact thrust ejected from the engine ranges as well. Figure 14 shows the ellipse created from uncertainties in the vertical direction from pointing and mounting inaccuracies of the engine as well as the variability in thrust exerted from the engine system in the horizontal direction.

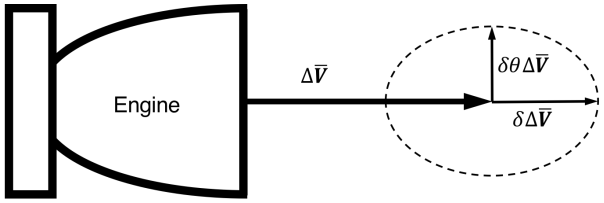

Figure 14: Each rocket engine comes with its own imperfections which include mounting error ($\delta\theta\bar{V}$) and thrust uncertainties ($\delta\bar{V}$).

The ellipse created in Figure 14 is formed from the uncertainties in the vertical and horizontal direction with respect to the engine and thrust. Mounting errors could point the $\Delta\bar{V}$ vector slightly upward, and using small angle approximation, the vertical component of the vector would be $\delta\theta\Delta\bar{V}$. As well, the engine could

provide slightly less or slightly more thrust than required of the maneuver from imperfections in hardware, resulting in the horizontal vector $\delta\Delta\bar{V}$. Together, these smaller vectors act as the semi-major and semi-minor axes of an ellipse that contains a distribution of points, which represent the likelihood of uncertainty in the final thrust vector.

This research takes into account degrees of mounting error with percent difference from nominal thrust. These effects individually and in combination are discussed later with respect to their effects on a trajectory.

B. Mathematical Derivations of Dynamics and Filtering

1. Circular Restricted Three-Body Problem

The Circular Restricted Three-Body Problem (CR3BP) is one method to represent a vehicle traveling within the Earth-Moon system. The following dynamics form the foundation for modeling the trajectories of the vehicle after aborting from circular orbit around the moon. The x, y, and z accelerations are:

$$\ddot{x} = 2\dot{y} + x(1-\mu)\frac{x+\mu}{\rho_1^3} - \mu\frac{x-1+\mu}{\rho_2^3} \tag{24}$$

$$\ddot{y} = -2\dot{x} + (1 - \frac{1-\mu}{\rho_1^3} - \frac{\mu}{\rho_2^3})y \tag{25}$$

$$\ddot{z} = -(\frac{1-\mu}{\rho_1^3} + \frac{\mu}{\rho_2^3})z \tag{26}$$

In the case of the Earth-Moon system, the mass ratio is 81.3 and is used to calculate μ and the x_1 and x_2 positions. These values also allow for the computation of each R_i:

$$\mu = \frac{m_2}{m_1 + m_2} \tag{27}$$

$$R_1 = \sqrt{(x+\mu)^2 + y^2 + z^2} \tag{28}$$

$$R_2 = \sqrt{(x-1+\mu)^2 + y^2 + z^2} \tag{29}$$

It can be shown that the use of the pseudo-potential Ω makes integration of the CR3PB easier. The following equations are the result of integrating Equations 24, 25, and 26 with respect to x, y, and z which gives:

$$\Omega_{x-dir} = \frac{x^2}{2} + \frac{1-\mu}{R_1} + \frac{\mu}{R_2} + f(y,z) \tag{30}$$

$$\Omega_{y-dir} = \frac{y^2}{2} + \frac{1-\mu}{R_1} + \frac{\mu}{R_2} + f(x,z) \tag{31}$$

$$\Omega_{z-dir} = \frac{1-\mu}{R_1} + \frac{\mu}{R_2} + f(x,y) \tag{32}$$

When all of these equations are combined, the final Ω solution is:

$$\Omega = \frac{1}{2}(x^2+y^2) + \frac{1-\mu}{R_1} + \frac{\mu}{R_2} \tag{33}$$

In order to use the Extended Kalman Filter, the state transition matrix (Φ or STM) is used, which satisfies:

$$\dot{\mathbf{\Phi}}(t,t_0) = \mathbf{A(x}(t))\mathbf{\Phi}(t,t_0) \tag{34}$$

The $A(x(t))$ matrix is composed of the partial derivatives as well.

$$A(t) = \frac{\partial \mathbf{X}(t)}{\partial \mathbf{X}(t_0)} \tag{35}$$

Specifically for the CR3BP, the $A(t)$ matrix is given as,

$$A(t) = \begin{bmatrix} 0 & I \\ \Omega_R & \Omega_V \end{bmatrix} \tag{36}$$

where Ω_R and Ω_V are the partial derivatives of the Ω equations with respect to position and velocity, respectively. Equation 37 shows how the $A(t)$ matrix is expanded, where the lower left quadrant (Ω_R) contains the partial derivatives of the Ω function with respect to position.

$$\mathbf{A}(\mathbf{x}(t)) = \begin{bmatrix} 0 & 0 & 0 & 1 & 0 & 0 \\ 0 & 0 & 0 & 0 & 1 & 0 \\ 0 & 0 & 0 & 0 & 0 & 1 \\ \Omega_{xx} & \Omega_{xy} & \Omega_{xz} & 0 & 2 & 0 \\ \Omega_{yx} & \Omega_{yy} & \Omega_{yz} & -2 & 0 & 0 \\ \Omega_{zx} & \Omega_{zy} & \Omega_{zz} & 0 & 0 & 0 \end{bmatrix} \tag{37}$$

The following equations represent the expanded partial derivatives of Ω with respect to each position variable, x, y, and z:

$$\Omega_x = x + \frac{(2\mu + 2x)(\mu - 1)}{2R_1^3} - \frac{\mu(2\mu + 2x - 2)}{2R_2^3} \tag{38}$$

$$\Omega_y = y - \frac{\mu z}{R_2^3} + \frac{y(\mu - 1)}{R_1^3} \tag{39}$$

$$\Omega_z = \frac{z(\mu - 1)}{R_1^3} - \frac{\mu z}{R_2^3} \tag{40}$$

As well, Equations 41 through 49 are the even further expanded equations that are in the lower left quadrant of the Jacobian matrix (Equation 37).

$$\Omega_{xx} = \frac{(\mu - 1)}{R_1^3} - \frac{\mu}{R_2^3} + \frac{3\mu(2\mu + 2x - 2)^2}{4R_2^5} - \frac{3(2\mu + 2x)^2(\mu - 1)}{4R_1^5} + 1 \tag{41}$$

$$\Omega_{xy} = \frac{3\mu y(2\mu + 2x - 2)}{2R_2^5} - \frac{3y(2\mu + 2x)(\mu - 1)}{2R_1^5} \tag{42}$$

$$\Omega_{xz} = \frac{3\mu z(2\mu + 2x - 2)}{2R_2^5} - \frac{3z(2\mu + 2x)(\mu - 1)}{2R_1^5} \tag{43}$$

$$\Omega_{yx} = \frac{3\mu y(2\mu + 2x - 2)}{2R_2^5} - \frac{3y(2\mu + 2x)(\mu - 1)}{2R_1^5} \tag{44}$$

$$\Omega_{yy} = \frac{\mu - 1}{R_1^3} - \frac{\mu}{R_2^3} - \frac{3y^2(\mu - 1)}{R_1^5} + \frac{3\mu y^2}{R_2^5} + 1 \tag{45}$$

$$\Omega_{yz} = \frac{3\mu yz}{R_2^5} - \frac{3yz(\mu - 1)}{R_1^5} \tag{46}$$

$$\Omega_{zx} = \frac{3\mu z(2\mu + 2x - 2)}{2R_2^5} - \frac{3z(2\mu + 2x)(\mu - 1)}{2R_1^5} \tag{47}$$

$$\Omega_{zy} = \frac{3\mu yz}{R_2^5} - \frac{3yz(\mu - 1)}{R_1^5} \tag{48}$$

$$\Omega_{zz} = \frac{\mu - 1}{R_1^3} - \frac{mu}{R_2^3} - \frac{3z^2(\mu - 1)}{R_1^5} + \frac{3\mu z^2}{R_2^5} \tag{49}$$

With this, the following expressions are used to solve for the State Transition Matrix over a set period of time. To start, the initial value of Φ, which is simply an identity matrix of $n \times n$ where $n = 6$ in this scenario given $x, y, z, \dot{x}, \dot{y}$, and $\dot{z}$.

$$\mathbf{\Phi}(t_0, t_0) = \mathbb{I}^{n\times n} = \mathbb{I}^{6\times 6} = \begin{bmatrix} 1 & 0 & 0 & 0 & 0 & 0 \\ 0 & 1 & 0 & 0 & 0 & 0 \\ 0 & 0 & 1 & 0 & 0 & 0 \\ 0 & 0 & 0 & 1 & 0 & 0 \\ 0 & 0 & 0 & 0 & 1 & 0 \\ 0 & 0 & 0 & 0 & 0 & 1 \end{bmatrix} \tag{50}$$

Equation 34 is then used in MATLAB to build the STM by using *ode*45.

C. Simulation and EKF Estimation Trajectory Sample Results

The trajectory propagation tool developed for this research was built in MATLAB and used six functions. A brief explanation of each function is provided in Appendix A. The general strategy of building the code involved two main parts: (1) development of a simulation for the trajectory of a vehicle with engine mounting and thrust errors built in and (2) an EKF estimation simulation using range measurements for corrections. The first simulation is referred to simply as "Simulation (Truth)" while the latter is "EKF Estimation". A range of simulations with various errors, measurement corrections, times between updates, etc. were tested in this analysis. The list of trajectories and their respective errors for the "Simulation (Truth)" is in Table 4. All EKF estimations were run using various sizes of time steps where measurements, and therefore corrections, were made.

Table 2: Example Abort Trajectory Options for Analysis.

Trajectory	Abort Strategy	Mounting Error (Degrees)			Thrust Error
		X	Y	Z	
0-ideal	Two-Impulse Example, Zero Errors	0.000	0.000	0.000	0%
0-N	Two-Impulse Example, Mounting Error	0.500	0.500	0.500	0%
0-TE+	Two-Impulse Example, Over-thrust	0.500	0.500	0.500	+1%
0-TE-	Two-Impulse Example, Under-thrust	0.500	0.500	0.500	-1%

The first simulation modeled was the two-impulse abort method, referred to as Trajectory 0. The vehicle starts in Low Lunar Orbit (LLO) at an altitude of 110 kilometers located along the vector connecting the Earth and Moon through their centers of mass. The vehicle trajectory is propagated one half orbit around the Moon before taking its first impulse on the dark side of the Moon. This puts the vehicle on a path away from the Moon where its next impulse is taken at the edge of the Moon's SOI. This last impulse places the vehicle on a trajectory to re-enter the Earth's atmosphere safely. The determination of "safe re-entry" was an estimation based on the angle at which the vehicle path made with the curve of the Earth; this was not an exact calculation of the flight path angle, γ. The entirety of the trajectory from LLO to Earth is plotted in Figure 15. Figure 16 shows the same trajectory near the Earth and the Moon. In Table 3, the description for Trajectory 0 is given with normalized position, velocity, and time all provided. Position and velocity are normalized by the distance between the Earth and the Moon while time is provided in hours.

Based on data from the Apollo 11 trajectory, Trajectory 0-ideal is longer than a nominal Apollo flight from the Earth to the Moon which means that the first impulse should have placed the vehicle on a more horizontal trajectory (less velocity in the y-direction) to reach Earth quicker. However, this trajectory is simply meant to be used as a tool to show how errors affect the trajectory and is not optimized for time of flight.

In each of the aforementioned Figures 15 and 16, there are two trajectories plotted. One (in black) is the simulation whereby thrust and engine mounting errors are taken into account with no maneuver corrections beyond the impulses. In red, however, is the EKF estimation of the trajectory which takes into account measurement corrections with each time step. The time steps are not equally spaced and are given as a user input within the simulation code. The vector of time steps in hours is given in Equation 51:

Table 3: Two-Impulse Trajectory Description.

Stage	Position			Impulse			Time Elapsed
	X	Y	Z	X	Y	Z	
Initial	0.983	0.000	0.000	-	-	-	0.000 hrs
Impulse 1	0.993	0.000	0.000	0.400	0.600	0.000	0.989 hrs
Impulse 2	0.841	0.079	0.000	-0.460	0.126	0.000	41.646 hrs
Arrive at Earth	-0.028	0.003	0.000	-	-	-	106.197 hrs

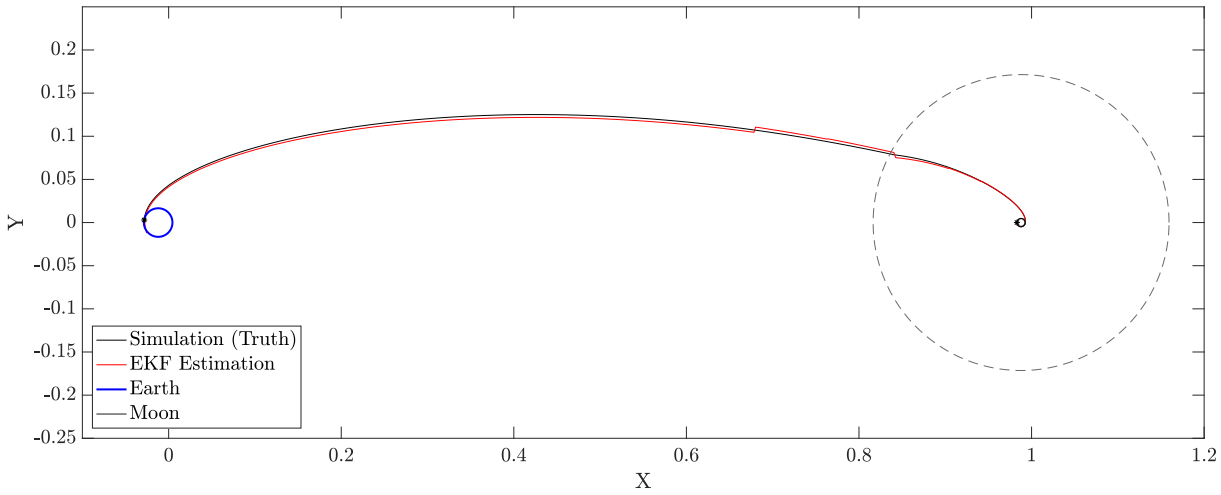

Figure 15: Ideal two-impulse abort trajectory (Trajectory 0-ideal in full).

$$t = \begin{bmatrix} 0 & 0.9891 & 10.4114 & 20.8229 & 41.6457 & 52.0571 & 62.4686 \end{bmatrix} \tag{51}$$

At each of these time steps, the EKF took range measurements in to correct the trajectory. This can sometimes be seen in a plot where a discontinuity occurs along the red EKF estimation trajectory. However, with small enough time steps, the two trajectories, truth and EKF, are nearly indistinguishable, as seen in the right image of Figure 16. Because the Simulation (Truth) has no engine mount or thrust errors and the EKF estimation uses the same dynamics, a lack of separation in the curves is understandable for this introductory example.

The longest time step for Trajectory 0 was roughly eleven hours, but the most noticeable offset between Simulation and EKF occurs in the left image of Figure 16. Here, the Simulation reaches the surface of Earth, but the EKF overshoots and given the allowed time to propagate, plunges through the Earth. This shows that while the last time step was only a ten hour gap and not the maximum step, the vehicle was traveling fast enough that the propagating error caused significant position differences in the end. Of note, the use of a random number generator in the code for representing noise in the measurement signal can cause the EKF to behavior differently with each trial run. Sometimes the EKF estimation undershoots the Simulation which implies the vehicle arrives at Earth's atmoshere at a higher flight path angle γ.

The next analysis on Trajectory 0 involves identifying changes to the trajectory when the errors are added to the system. First, engine mounting errors were added in. One half degree of mounting error in each direction is taken into account using a rotation matrix which shifts the thrust vector slightly using the small angle approximation. It is estimated that one half degree is the maximum obtainable accuracy with which a rocket can be mounted, therefore, one half degree of misalignment in each direction is taken as the nominal rocket engine mounting error. As previously mentioned, these angles of misalignment are put into a

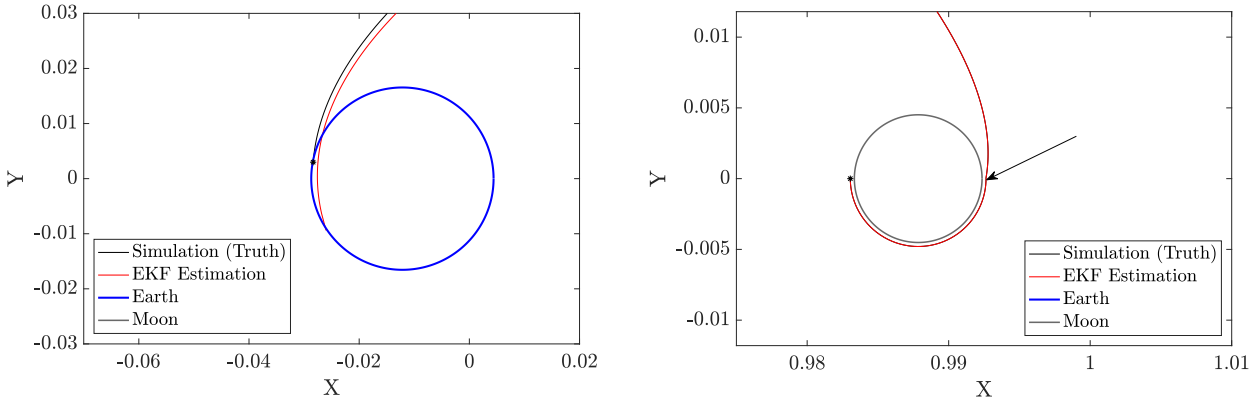

Figure 16: Trajectory 0-ideal at Earth and the Moon. The arrow in the right image of the figure designates the location of the first impulse at the Moon.

rotation matrix which then calculates the resultant thrust vector direction using small angle approximations. These mounting errors are only used during an impulse. To see how this mounting error affects the ideal trajectory, they are plotted together in Figure 17.

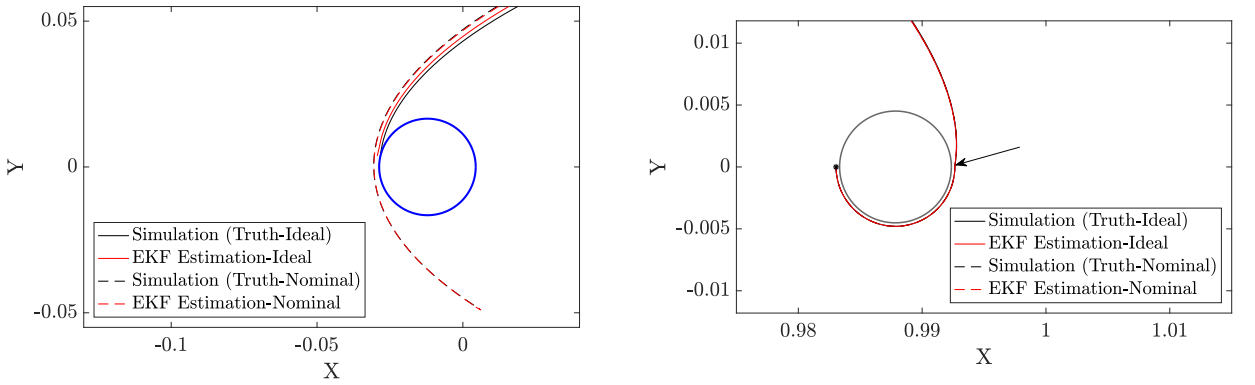

Figure 17: Trajectory 0-Ideal and Trajectory 0-Nominal plotted together to display how the affects of engine mounting change the end destination of the vehicle. The arrow in the right image points to the location where an impulse was completed.

From Figure 17, it is clear that near the Moon, the mounting errors do not affect the trajectory on a relevant scale, but when left to propagate, these errors are detrimental to reaching the Earth. FIgure 17 shows that the nominak thrust error with errors built in overshoots the Earth when using the same impulse schedule as the ideal case. Fortunately, it is most likely that this misalignment would be well understood and taken care of given engine burns early in the mission. However, should an abort take place for an engine-related hardware issue, any original burn calculations using the nominal engine misalignment would

result in an incorrect trajectory to reach Earth.

The variability in thrust for each burn must also be taken into account whereby more or less thrust than expected can affect the final position of the vehicle. Three different thrust magnitudes were used in propagating Trajectory 0, namely 0-TE+ and 0-TE-, where thrust error varied by one percent of nominal, but no engine alignment errors were used. For these two thrust error scenarios, Figure 18 shows how the trajectories under- and overshoot the Earth from nominal. To avoid overcrowding on the plots, the EKF estimations are not shown.

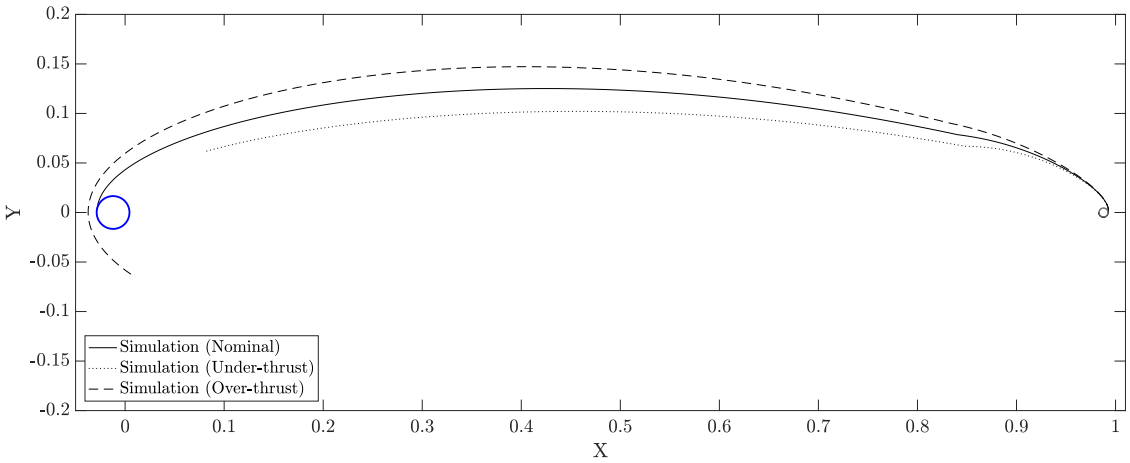

Figure 18: Trajectory 0-Ideal plotted with varying thrust errors of over and under one degree from nominal expected thrust during impulse maneuvers.

Interestingly, for this two-impulse case, an over-performing engine has a much more dire result than under-performing one. Figure 18 reveals that while neither option is ideal, a thruster operating at 99% power gets the vehicle close to the nominal trajectory, albeit a shallower path, but the nominal 106-hour travel time is not enough. A slight course correction and longer flight time is required to reach Earth. However, the over-performing engine completely misses the Earth and would require a more major course correction and longer orbit time around Earth to slow down and re-enter the atmosphere. The encouraging result here is that odds are low that an engine would over-perform if hardware malfunctions occur on the vehicle. This means that an impulse slightly less than expected could be fixed with small course corrections mid-flight if the capability still existed to execute such a correction. Figure 18 also shows that when the thrust is not nominal, the second impulse of the maneuver does not occur at the edge of the Moon's SOI. This is intuitive given that the time steps for when the impulses occurred remained the same while their magnitudes were slightly different, meaning not only may Mission Control need to adjust their impulse magnitudes in an abort, but they also may need to adjust the impulse schedule (location and time of an impulse) as well.

D. Abort Trajectory Simulation and Comparison

Now that the effects of engine misalignment and thrust magnitude differences have been taken into affect with a sample trajectory, the same effects will be analyzed and compared for the one- and three-impulse abort strategies. Because the sample used two impulses, this abort strategy was not reanalyzed. Table 4 outlines the comparisons that are made between each trajectory strategy.

The nominal single-impulse trajectory (Trajectory 1-N) is seen in-full in Figure 19a and again in Figure 19b where the trajectory near the Earth and the Moon can be seen. The vehicle orbits three quarters of the way around the Moon before a single burn to return to Earth. Compared to Trajectory 0, Trajectory 1-N has a more horizontal path which forces the vehicle to return to Earth in the opposite orientation around Earth from the sample trajectory in Figure 15; Trajectory 0 returns "from above" while Trajectory 1-N approaches Earth "from below." Only one major measurement correction discontinuity can be see in Figure 19a which

Table 4: Example Abort Trajectory Options for Analysis.

Trajectory	Abort Strategy	Mounting Error (Degrees)			Thrust Error
		X	Y	Z	
1-N	One-Impulse Abort, Nominal Thrust	0.500	0.500	0.500	0%
1-TE+	One-Impulse Abort, Over-thrust	0.500	0.500	0.500	+1%
1-TE-	One-Impulse Abort, Under-thrust	0.500	0.500	0.500	-1%
3-N	Three-Impulse Abort, Nominal Thrust	0.500	0.500	0.500	0%
3-TE+	Two-Impulse Abort, Over-thrust	0.500	0.500	0.500	+1%
3-TE-	Two-Impulse Abort, Under-thrust	0.500	0.500	0.500	-1%

occurs near $x = 0.9$. While the EKF estimation undershoots the Simulation re-entry location, Figure 19a shows that only a small last minute correction of the EKF would improve the estimation. For the most part, however, the EKF estimation does an excellent job of keeping up with the Simulation trajectory. Table 5 provides the impulse schedule with the time elapsed to reach Earth. The single-impulse abort only took 64 hours compared the Trajectory 0's (a two-impulse abort strategy) 106-hour travel time.

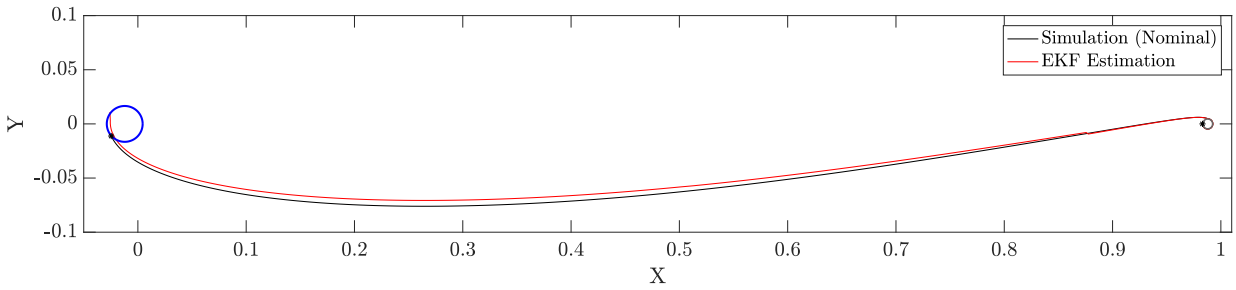

(a) Full view of single-impulse nominal trajectory.

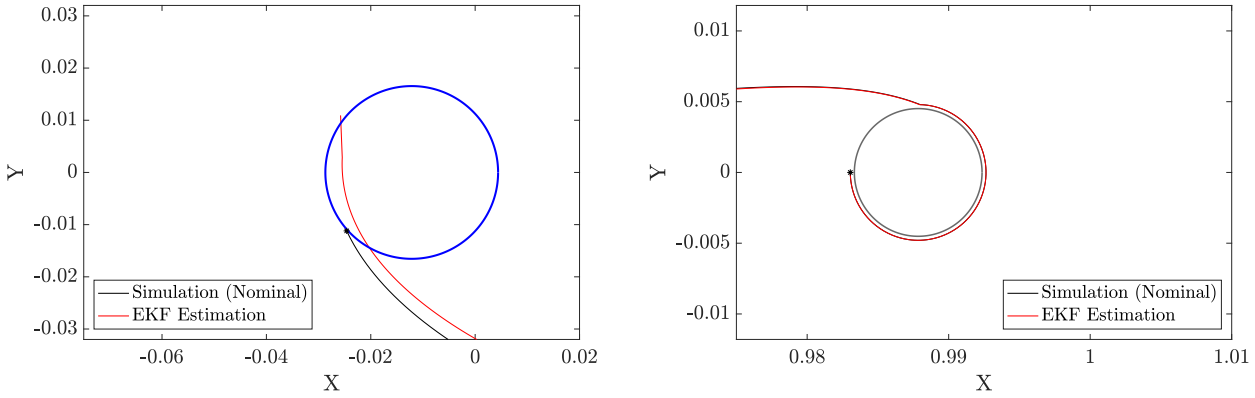

(b) Single-impulse nominal trajectory shown near the Earth and the Moon.

Figure 19: Single-impulse nominal trajectory with engine mounting errors included.

It was then modeled to see how thrust magnitude errors change this single-impulse nominal trajectory; the results of such modeling are in Figure 20. Unlike Trajectory 0's over-thrust results where the vehicle overshot Earth by a wide margin, Trajectory 1–TE+ forced the trajectory onto a more horizontal path which resulted in a steep flight path angle, which would result in over-heating on re-entry. However, both Trajectories 1–TE+ and 1–TE- have a much narrower spread compared to the same thrust magnitude errors propagated in

Table 5: Single-Impulse Trajectory Description.

Stage	Position			Impulse			Time Elapsed
	X	Y	Z	X	Y	Z	
Initial	0.983	0.000	0.000	-	-	-	0.000 hrs
Impulse 1	0.988	0.005	0.000	-0.71	0.88	0.000	1.468 hrs
Arrive at Earth	-0.025	-0.011	0.000	-	-	-	64.113 hrs

Trajectory 0–TE+ and 0–TE-. This can be attributed to the large x-component that dominates the velocity vector. Because of this concentration of the impulse in the x-direction, the thrust error propagates less in the y-direction away from the path of Trajectory 1-N.

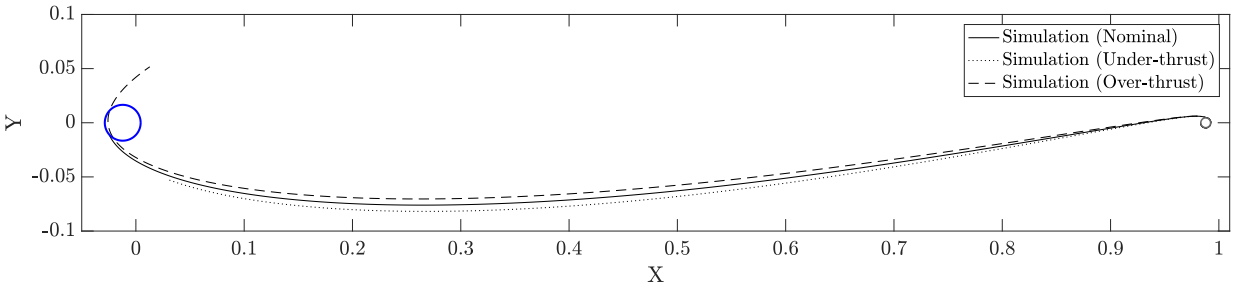

Figure 20: Single-impulse nominal trajectory 1-N plotted against 1–TE+ and 1–TE- to show how thrust magnitude differences propagate across the same planned trajectory.

Next, the three-impulse maneuver was analyzed; Table 6 describes the maneuver and its execution while Figure 21 displays the trajectory in full as well as near the Earth and the Moon. The three-impulse strategy begins by impulsing immediately from the position in LLO where the vehicle lies on the vector connecting the Earth and Moon via their centers of mass. Once the impulse is taken, the vehicle orbits to the opposite side of the Moon to perform a second impulse burn placing the vehicle on a trajectory towards Earth. The last burn takes place at the edge of the Moon's SOI to propel the vehicle on a trajectory that allows for a shallow flight path angle to re-enter the Earth's atmosphere.

Table 6: Three-Impulse Trajectory Description.

Stage	Position			Impulse			Time Elapsed
	X	Y	Z	X	Y	Z	
Initial	0.000	0.983	0.000	-	-	-	0.000 hrs
Impulse 1	0.000	0.983	0.000	0.000	-0.50	0.00	0.000 hrs
Impulse 2	1.018	0.000	0.000	-0.40	0.55	0.00	6.819 hrs
Impulse 3	0.823	0.046	0.000	-0.71	0.18	0.00	37.481 hrs
Arrive at Earth	-0.020	0.020	0.000	-	-	-	97.690 hrs

Similar to the 1-N plot, Trajectory 3-N shows that even with long periods between measurements (the most being 60 hours), the EKF does predict the trajectory well albeit with some slight overshoot. With some extra time to propagate, the EKF would also reach a re-entry point around the Earth.

The more curious results came when observing how thrust magnitude errors affect the three-impulse trajectory. Figure 22 demonstrates that under-performing engine burns do not always result in a shorter trajectory for a given time. In the case of this three-impulse abort, if the engine performs at 99% thrust, the vehicle overshoots the Earth and has a larger flight path angle, which is detrimental to a safe re-entry. Trajectory 3–TE- also is propagated for too long; this is the opposite result from Trajectory 1–TE- in Figure

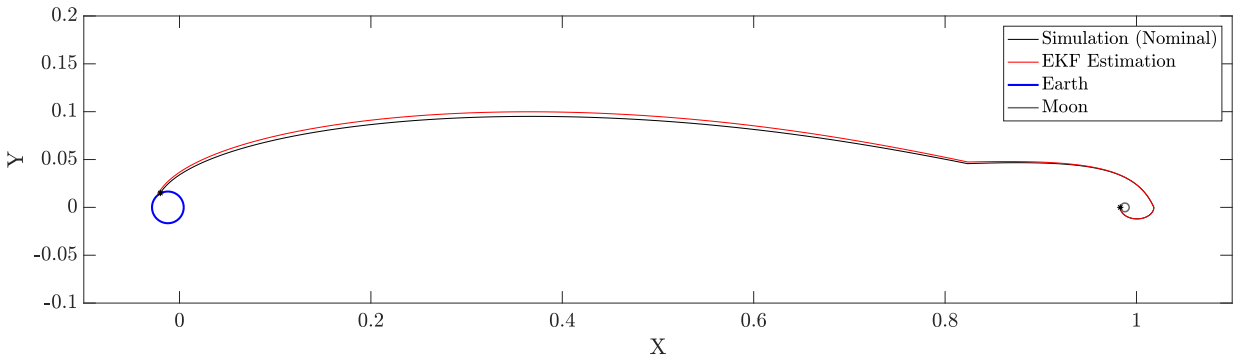

(a) Full view of three-impulse nominal trajectory.

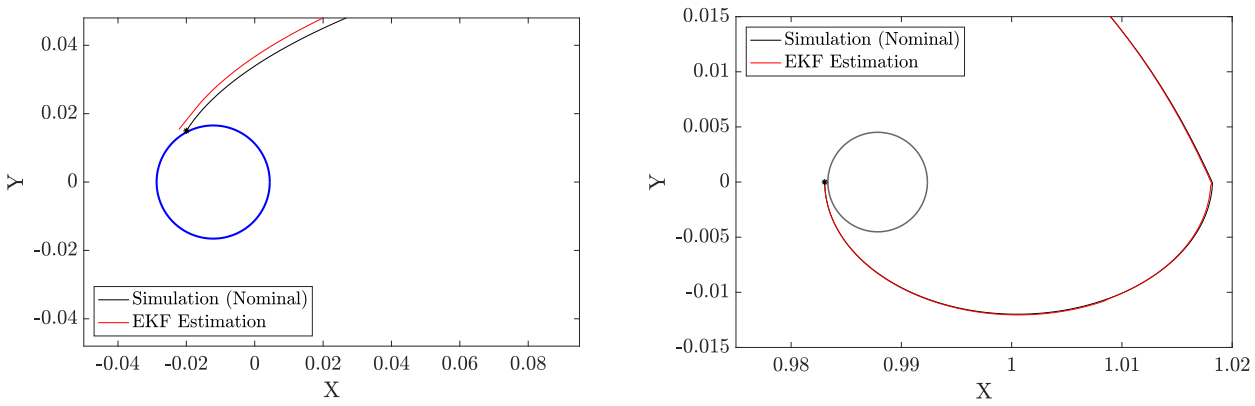

(b) Three-impulse nominal trajectory shown near the Earth and the Moon.

Figure 21: Three-impulse nominal trajectory with engine mounting errors included.

20. This occurs because of the convexity of the trajectory with respect to the XY-plane used in the figures of this paper. A convex trajectory like the single-impulse Trajectory 1–TE- shows that an under-performing engine will take longer to reach Earth compared to the nominal abort while the concave Trajectory 3–TE- requires less time to reach Earth but at the expense of a higher flight path angle γ.

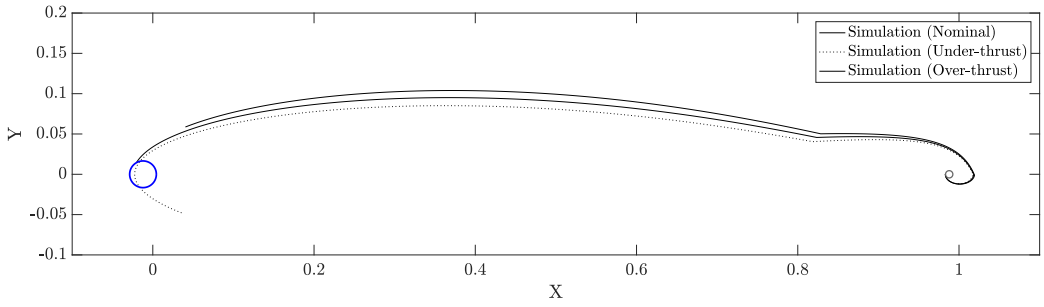

Figure 22: Three-impulse nominal trajectory 3-N plotted against 3–TE+ and 3–TE- to show how thrust magnitude differences propagate across the same planned trajectory.

This is an important consideration when planning for an abort. As seen between the three abort strategies modeled in this section, the starting point from which an abort takes place as well as the number of engine burns required will change how the vehicle approaches Earth. This convexity change (which results in either a prograde or retrograde entry into Earth's atmosphere) is an important consideration when comparing

abort options and the root cause of the abort (hardware, crew health, etc.). This factor of convexity must therefore be taken into account just as time of flight and fuel remaining were in Sections IV and V.

Furthermore, the flight time for Trajectory 3-N was 97 hours which is shorter than Trajectory-0 used two impulses. This means that Trajectory 0 was not optimized to have a flight time of less than 97 hours (but greater than Trajectory 1-N's time of 64 hours), which was an important result from Section V. This means that more investigation must be done to see if the optimized trajectories for each impulse means the longest time of flight belongs to the trajectory with the most impulses.

VII. Conclusion

This research aimed to investigate manned mission aborts from lunar orbit and provide an outline of abort strategies given a mission planner's inputs. This work combined two historical papers and their respective methods by focusing on one-, two-, and three-impulse aborts to leave the Moon and lunar orbit to return to Earth. While some reconciling was needed to compare the results of each, the Gunther and Edelbaum methods worked well in determining which abort strategy was more fuel efficient. The final results showed that each method had an optimized solution given nominal information about the lunar orbit of the space vehicle. The single-impulse abort method was optimal at very high values of K, or normalized V_∞. On the contrary, the two-impulse abort was best if the desired K were mid-range, while the three-impulse abort favored at low values of K.

For the trajectory modeling and EKF estimation, it was clear that the EKF measurement updates could be fairly infrequent over the trip and guarantee that the estimation matched the simulation truth well. With respect to abort strategies, this analysis revealed that the convexity or concavity of the trajectory play an important role in determining which abort should be chosen based on the engine performance. If a burn is not guaranteed to be at nominal and may under-perform, the three-impulse maneuver may provide a trajectory that results in a steeper flight path angle causing the vehicle to burn up on re-entry. This finding means that "convexity" is a factor as important as time of flight and fuel required for the abort.

Future work that would expand upon this investigation could easily extend this analysis to incorporate a better tool or simulation for estimating time of flight of the vehicle. Because the Edelbaum and Gunther derivations focused mostly on quantities of velocity and position rather than their vector forms, many of the trajectories plotted were not optimized for time of flight. It would be worthwhile to propagate the trajectories with Edelbaum and Gunther's magnitudes and solve for the vector direction simultaneously to use in the trajectory modeling. Using limitations in fuel would also increase the usefulness of this analysis to limit the trajectories to only those obtainable by fuel remaining on-board the vehicle.

References

[1] XiaoNing Xi, WenDe Huang, and Wei Wang. Review on abort trajectory for manned lunar landing mission. *Science China Technological Sciences*, 53(10):2691–2698, October 2010.

[2] WenDe Huang, XiaoNing Xi, and Wei Wang. Characteristic analysis and design of near moon abort trajectory for manned lunar landing mission. *Science China Technological Sciences*, 53(11):3129–3137, November 2010.

[3] E. Beksinski. Abort trajectories for manned lunar missions, January 2007.

[4] Craig A Kluever and Bion L Pierson. Optimal low-thrust three-dimensional earth-moon trajectories. *Journal of Guidance, Control, and Dynamics*, 18(4):830–837, 1995.

[5] NASA. *Space Launch System highlights*. 2012.

[6] US Congress. *An update on the Space Launch System and Orion monitoring the development of the nation's deep space exploration capabilities : hearing before the Subcommittee on Space, Committee on Science, Space, and Technology, House of Representatives, One Hundred Thirteenth Congress, second session, December 10, 2014*. 2015.

[7] Sheng-ping Gong, Jun-feng Li, He-xi Baoyin, and Yun-feng Gao. Lunar landing trajectory design based on invariant manifold. *Applied mathematics and mechanics*, 28(2):201–207, 2007.

[8] Ronald R Sostaric and Robert S Merriam. Lunar ascent and rendezvous trajectory design. 2008.

[9] D Harold Shelton. Apollo experience report: Guidance and control systems. lunar module stabilization and control system. 1975.

[10] Daniel R Adamo. Apollo 13 trajectory reconstruction via state transition matrices. *Journal of guidance, control, and dynamics*, 31(6):1772–1781, 2008.

[11] P Gunther. Asymptotically optimum two-impulse transfer from lunar orbit. *AIAA Journal*, 4(2):346–352, 1966.

[12] TN Edelbaum. Optimal nonplanar escape from circular orbits. *AIAA Journal*, 9(12):2432–2436, 1971.

[13] Shane Robinson and David Geller. A simple targeting procedure for lunar trans-earth injection. In *AIAA Guidance, Navigation, and Control Conference*, page 6107, 2009.

[14] AIAA 8th Aerospace Sciences Meeting. *Launch Window and Translunar, Lunar Orbit, and Transearth Trajectory Planning and Control for the Apollo 11 Lunar Landing Mission*, 1290 Avenue of the Americas, New York, NY 10019, January 1970.

[15] Colorado Center for Astrondynamics Research University of Colorado. Interplanetary mission design.

Appendix A Trajectory Propagation Code Summary

The following functions were used to propagate the trajectories for a simulated truth with engine mounting error and thrust magnitude error as well as an Extended Kalman Filter with range measurement updates. Each function description is provided.

1. **Sim_dynamics.m**

   Dynamics of CR3BP using pseudo-potential function in Earth/Moon system that compiles "f_out" to be integrated

2. **Sim_StateProp.m**

   Uses ode45 to propagate the Sim_dynamics.m of the system

3. **EKF_dynamics.m**

   Uses dynamics of the CR3BP to build the State Transition Matrix, Covariance Matrix, and f_out vector for integration

4. **EKF_StateEstProp.m**

   Uses ode45 to propagate the EKF_dynamics.m which propagates the dynamics and the covariance matrix

5. **EKF_Correction.m**

   Calculates the Kalman Gain, State Estimate Update, and Covariance Update for each dt time segment

6. **measurement.m**

   Calculation of the range measurement from an Earth-based system to update the EKF_Correction.m function